Journal of Ovarian Research

RESEARCH

Open Access

# Sterigmatocystin declines mouse oocyte quality by inducing ferroptosis and asymmetric division defects

Shiwei Wang[1,3†], Xuan Wu[1,3†], Juan Yang[1], Yuwan Peng[1], Fulu Miao[1], Min Li[1] and Juan Zeng[1,2*]

## Abstract

**Background** Sterigmatocystin (STE) is a mycotoxin widely found in contaminated food and foodstuffs, and excessive long-term exposure to STE is associated with several health issues, including infertility. However, there is little information available regarding the effects of STE toxin on the female reproductive system, particularly concerning oocyte maturation.

**Methods** In the present study, we investigated the toxic effects of STE on mouse oocyte maturation. We also used Western blot, immunofluorescence, and image quantification analyses to assess the impact of STE exposure on the oocyte maturation progression, mitochondrial distribution, oxidative stress, DNA damages, oocyte ferroptosis and asymmetric division defects.

**Results** Our results revealed that STE exposure disrupted mouse oocyte maturation progression. When we examined the cellular changes following 100 μM STE treatment, we found that STE adversely affected polar body extrusion and induced asymmetric division defects in oocytes. RNA-sequencing data showed that STE exposure affects the expression of several pathway-correlated genes during oocyte meiosis in mice, suggesting its toxicity to oocytes. Based on the RNA-seq data, we showed that STE exposure induced oxidative stress and caused DNA damage in oocytes. Besides, ferroptosis and α-tubulin acetylation were also found in STE-exposed oocytes. Moreover, we determined that STE exposure resulted in reduced RAF1 protein expression in mouse oocytes, and inhibition of RAF1 activity also causes defects in asymmetric division of mouse oocytes.

**Conclusions** Collectively, our research provides novel insights into the molecular mechanisms whereby STE contributes to abnormal meiosis.

**Keywords** Sterigmatocystin, RAF1, Oxidative stress, Ferroptosis, Oocyte

†Shiwei Wang and Xuan Wu contributed equally to this work.

*Correspondence:
Juan Zeng
juanzeng2023@163.com
[1]Department of Obstetrics and Gynecology, The First Affiliated Hospital of Anhui Medical University, No 218 Jixi Road, Heifei, Anhui 230022, China
[2]NHC Key Laboratory of Study on Abnormal Gametes and Reproductive Tract (Anhui Medical University), No 81 Meishan Road, Hefei 230032, China
[3]College of Animal Science and Technology, China Agricultural University, Beijing, China

## Introduction

The prerequisite to obtaining a healthy embryo is the production of a high-quality oocyte [1], and oocyte maturation with appropriate meiotic resumption is important for the acquisition of high-quality oocytes [2]. In mammalian oocytes, meiotic maturation is characterized by an asymmetric division, which produces a large egg and a small polar body [3]. In order to maintain maternal stores, oocytes expel a minimal amount of cytoplasm with half chromosomes, which is essential to the early embryonic development [4]. In addition, mammalian oocyte maturation is characterized by multi-stage, accurately orchestrated and systematic process [5]. As a hallmark of meiotic resumption, germinal vesicle breakdown (GVBD) represents the initiation of oocyte maturation [6]. After GVBD, the first meiotic spindle is assembled at the center of the oocyte and subsequently migrates to one side where an actin-rich cortical domain is formed that overlies the metaphase I (MI) spindle [7]. The spindle subsequently migrates to the cortex, and first polar body (Pb1) extrusion takes place, with the oocyte reaching and remaining at the metaphase II (MII) stage until fertilization [8].

There is an extensive and serious problem of mycotoxins contaminating food in many countries, particularly developing countries [9]. Sterigmatocystin (STE) is a common food contaminant produced by fungi and exerts potently negative economic effects on the biotechnological, agricultural, and food industries [10]. The mycotoxin STE is produced principally by *Aspergillus* fungi [11] and is hepatotoxic and nephrotoxic in animals; given this, STE has been classified as a possible human carcinogen (group 2B) by the International Agency for Research on Cancer [12, 13]. There are indications that dairy cattle suffer from diarrhea and death as a result of substantial levels of STE in their feed [14]. Epidemiological evidence also highlights the existence of associations between STE exposure and the risk of cancer development [12]. In vivo studies have revealed that STE induces tumors in several species of animals such as mice [15], rats [16], monkeys [17], and fish [18]. Exposure to STE has been additionally shown to induce oxidative stress-related impairment in rat liver and kidneys [19]. STE has been reported to markedly reduce cell proliferation in different mammalian cells [20] and can generate genotoxicity as it is able to form DNA-adducts and induce DNA damage [21]. Elevated incidence rates for liver and stomach cancers have been reported in areas with high levels of STE contamination [22]; teratogenic effects, embryonic morality, and embryonic developmental disorders resulting from STE exposure have been reported in chickens [23]. Nonetheless, the effects and underlying mechanisms of STE exposure on oocytes remain unclear.

In light of this, the aim of the present study was to investigate the negative effects of STE on the maturation progress of mouse oocytes. We assessed several critical indicators during oocyte nuclear and cytoplasmic maturation such as first polar body extrusion, defects in asymmetric division, cytoskeletal assembly, and oxidative stress.

## Results

### STE toxin exposure reduces the polar body extrusion rate of mouse oocytes

Oocytes were collected from adolescent mice that had been injected with PMSG 48 h previously. The collected oocytes were then cultured in M16 medium for 3, 8, and 14 h, by which time they had reached the germinal vesicle breakdown (GVBD), metaphase I (MI), and metaphase II (MII) stages, respectively. To study the STE toxicity on mice oocyte maturation progress, five groups of oocytes were treated with a concentration gradient of STE solution: 0 μM, 25 μM, 50 μM, 100 μM and 200 μM. We selected oocytes cultured in vitro for 14 h to observe the first polar body (Pb1) extrude, as shown in Fig. 1A, we noted that almost all oocytes matured and extruded their first polar body in the control group, however, exposure to STE inhibited oocyte maturation. Compared with the control group (82.7±3.68% [number of replicates=3, number of oocytes=145, and number of mice=6, $p<0.01$]), the PB1 extrusion rates were markedly declined after STE treatment in a dose-dependent manner. And the proportion of PB1 was 53.0±6.16% [number of replicates=3, number of oocytes=132, and number of mice=6], 44.2±5.14% [number of replicates=3, number of oocytes=157, and number of mice=6], 37.5±4.08% [number of replicates=3, number of oocytes=128, and number of mice=6], 35.0±4.08% [number of replicates=3, number of oocytes=116, and number of mice=6] in 25 μM, 50 μM, 100 μM and 200 μM STE groups (Fig. 1A and B), respectively. We also observed a large proportion of oocytes that extruded first polar body (Pb1) that was larger than 1/3 of the oocyte's diameter in the 100 μM treated oocytes compared with other group oocytes at the MII stage (Fig. 1C). The large polar body and symmetric division of oocytes constituted the chief phenotype related to failure of spindle migration during meiosis I [24]. These results suggested that STE caused the failure of oocyte maturation and induced the asymmetric division defects. For subsequent experiments, we chose 100 μM STE was chosen as the treatment concentration.

### RNA sequencing for the STE-exposed oocytes

We attempted to explore the potential mechanism of STE toxicity on mice oocyte maturation through RNA sequencing. Considering that oocytes cultured for 8 h

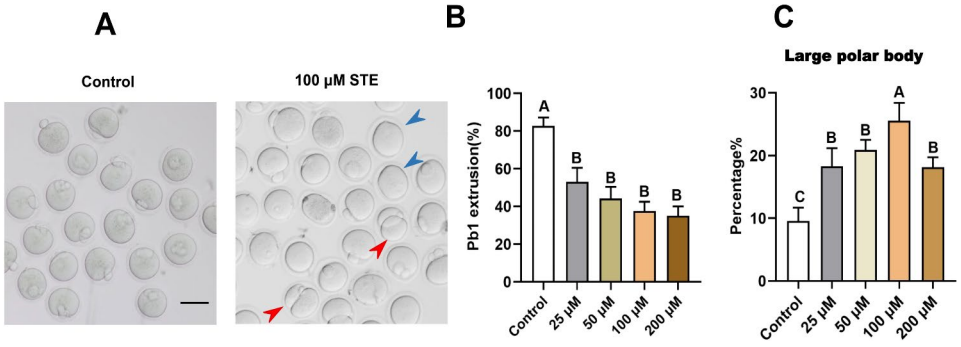


**Fig. 1** Effects of STE on maturational competence of mouse oocytes. (**A**) Representative images of oocytes from control and STE-treated groups. Red arrowheads denote oocytes with apparent symmetrical division and blue arrowheads indicate oocytes that fail to extrude polar bodies (scale bar, 80 μm). (**B**) The rate of polar body extrusion was significantly lower after STE exposure than in the control group. And the proportion of PB1 was (82.7 ± 3.68% [number of replicates = 3, number of oocytes = 145, and number of mice = 6], 53.0 ± 6.16% [number of replicates = 3, number of oocytes = 132, and number of mice = 6], 44.2 ± 5.14% [number of replicates = 3, number of oocytes = 157, and number of mice = 6], 37.5 ± 4.08% [number of replicates = 3, number of oocytes = 128, and number of mice = 6], 35.0 ± 4.08% [number of replicates = 3, number of oocytes = 116, and number of mice = 6], $p < 0.01$) in control, 25 μM, 50 μM, 100 μM and 200 μM STE groups, respectively. (**C**) The percentage of oocytes with large polar bodies after STE-treated. And the proportion of large polar body was (9.6 ± 1.72% [number of replicates = 3, number of oocytes = 145, and number of mice = 6], 18.3 ± 2.35% [number of replicates = 3, number of oocytes = 132, and number of mice = 6], 20.9 ± 1.31% [number of replicates = 3, number of oocytes = 157, and number of mice = 6], 25.6 ± 2.33% [number of replicates = 3, number of oocytes = 128, and number of mice = 6], 18.1 ± 1.32% [number of replicates = 3, number of oocytes = 116, and number of mice = 6], $p < 0.01$) in control, 25 μM, 50 μM, 100 μM and 200 μM STE groups, respectively. The Figure depicts the mean percentage ± SD of the results obtained from three independent experiments. The bars labeled with completely different letters indicate significant difference at $p < 0.01$

in vitro represents an intermediate stage between meiosis recovery (GVBD) and meiosis maturation (MII), the changes of oocytes at this stage will have an impact on the first polar body extrusion, so we chose to observe oocytes cultured for 8 h in vitro. The control and STE group oocytes were cultured in medium without or containing 100 μM STE, and oocytes were collected after 8 h of culture. Each group has 3 replicates, 40 oocytes (derived from 2 mice) per replicate. As the results shown in Fig. 2A and B, transcriptome analysis showed a total of 357 genes expression were changed due to 100 μM STE treatment compared with the control group. Among these genes with altered expression, 229 (60.15%) genes were upregulated, nevertheless, 128 (35.85%) genes were downregulated. In addition, we conducted GO term analysis on these differentially expressed genes. And the results showed that STE exposure mainly affected the metabolic process, intracellular component, and RNA binding function (Fig. 2C). Moreover, as shown in Fig. 2D and Supplementary Material 1, the results for KEGG pathway analysis indicated that STE exposure significantly affected the fatty acid biosynthesis (*Acsl4*, *Fasn*), fatty acid metabolism (*Acsl4*, *Scd3*, *Hacd4*, *Fasn*), ferroptosis (*Acsl4*, *Ncoa4*), cell cycle (*Ywhah*, *Ccnb1*, *Ccnh* and *Cdc25a*), and regulation of actin cytoskeleton (*Vav3*, *Mos*, *Raf1* and *Pik3cd*). Collectively, the results for RNA-seq provided the possible mechanisms for the STE toxicity on oocyte meiosis.

### STE causes mitochondrial distribution and membrane-potential defects in oocytes

We first assessed the effects of STE on mitochondria-related functions in oocytes. MitoTracker was deployed to evaluate the distribution of mitochondria in oocytes that at the 8 h of the IVM (in vitro maturation). Based on fluorescence staining, mitochondria accumulated at the spindle periphery in control oocytes, while the mitochondrial distribution was principally scattered or aggregated in clumps in the cytoplasm of the oocytes treated with STE (Fig. 3A). It was also apparent that the proportion of mitochondria surrounding the spindle in oocytes at the MI stage was lower than that in the control group (control group, 25.3±2.87% [number of replicates=3, number of oocytes=51, and number of mice=3]; STE group, 55.4±9.09% [number of replicates=3, number of oocytes=65, and number of mice=3]; $p<0.01$) (Fig. 3B). From the aforementioned results, we discerned that STE affected the mitochondrial distribution in MII oocytes. To determine whether STE also exerted toxic effects on the mitochondrial function of oocytes, we selected JC-1 as the membrane-potential stain to detect alterations in oocyte mitochondrial membrane potential. As shown in Fig. 3C, the fluorescence intensity of the red channel with mitochondria JC-1 in the STE group decreased relative to the control group, while the intensity of the green channel increased. We calculated the ratio of the red-to-green channel fluorescence intensity in the control and STE groups, and the data confirmed these findings (control group, 1.08±0.10 [number of replicates=3, number of oocytes=43, and number of mice=4]; STE group, 0.54±0.14 [ number of replicates=3, number of

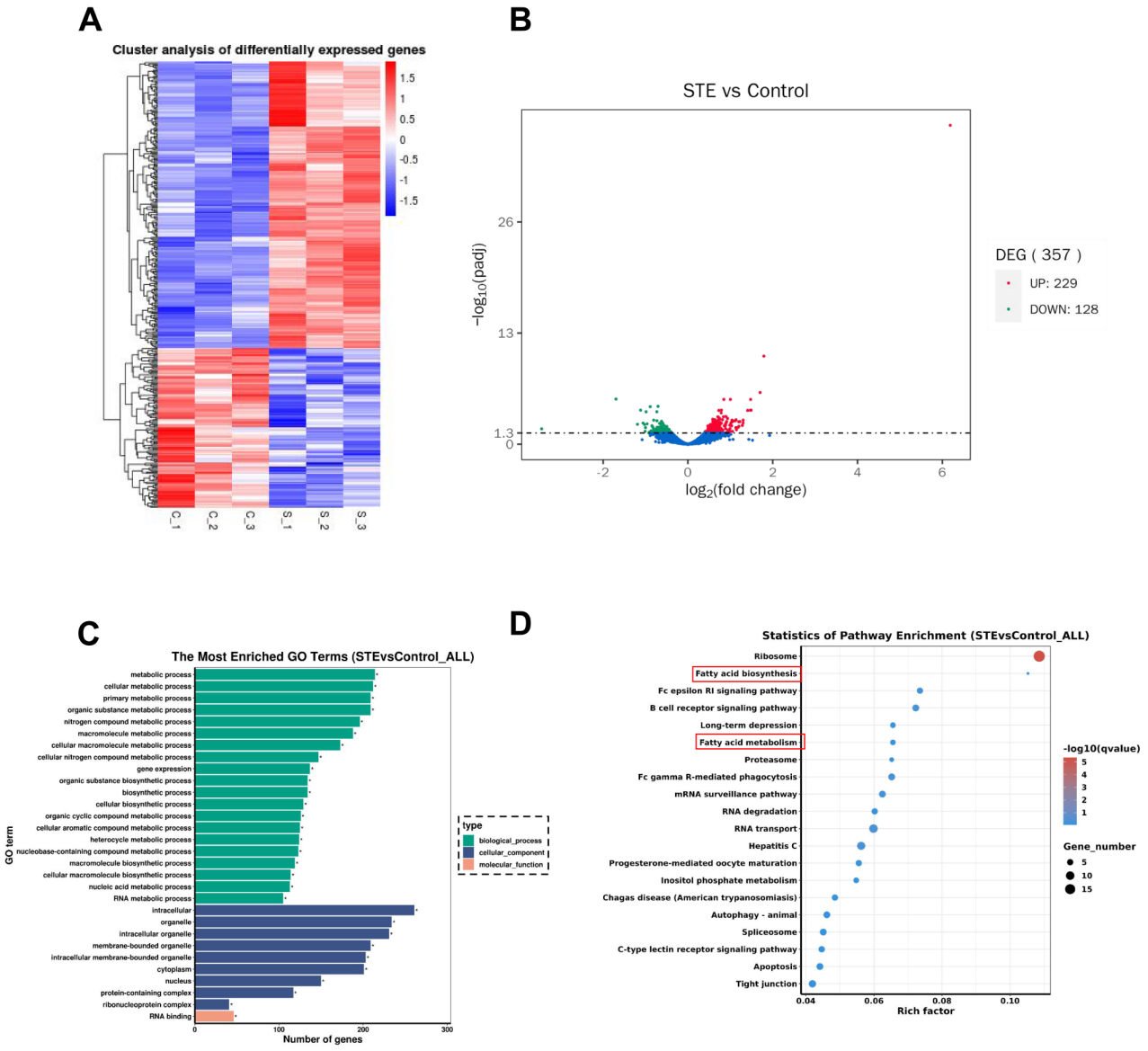


**Fig. 2** Transcriptome analysis for the effects of STE exposure on oocyte maturation. (**A**) The heat map for the altered expressed genes after STE treatment. (**B**) The numbers of altered expressed genes and volcano plot analysis after STE exposure. (**C**) The differential gene GO enrichment analysis for the differentially expressed genes after STE treatment. (**D**) The KEGG pathway enrichment analysis for the differentially expressed genes after STE exposure

oocytes=51, and number of mice=4]; $p<0.01$) (Fig. 3D). These results revealed that STE was toxic to the mitochondrial functions of oocytes.

### Exposure to STE toxin induces an increase in oxidative stress and DNA damage in mouse oocytes

Next, we investigated whether STE exposure influenced ROS levels in mouse oocytes. To address this line of inquiry, oocytes cultured for 8 h in vitro (MI) were collected from the control and STE-treatment groups and stained with CM-H2DCFDA fluorescent dye for the assessment of ROS generation. Compared with the control group, STE treatment significantly augmented the levels of ROS in mouse oocytes (Fig. 4A) as determined by mean fluorescence intensity (control group, 19.5±2.95 [number of replicates=3, number of oocytes=32, and number of mice=3]; STE group, 58.3±2.98 [number of replicates=3, number of oocytes=38 and number of mice=3]; $p<0.01$) (Fig. 4B). These findings implied that STE exposure disrupted redox homeostasis during oocyte maturation.

We also assessed the level of DNA damage by γ-H2AX staining of STE-exposed GV oocytes since excessive ROS may attack macromolecules in cells (including DNA). Additionally, our fluorescence imaging and intensity measurement data revealed that STE exposure generated

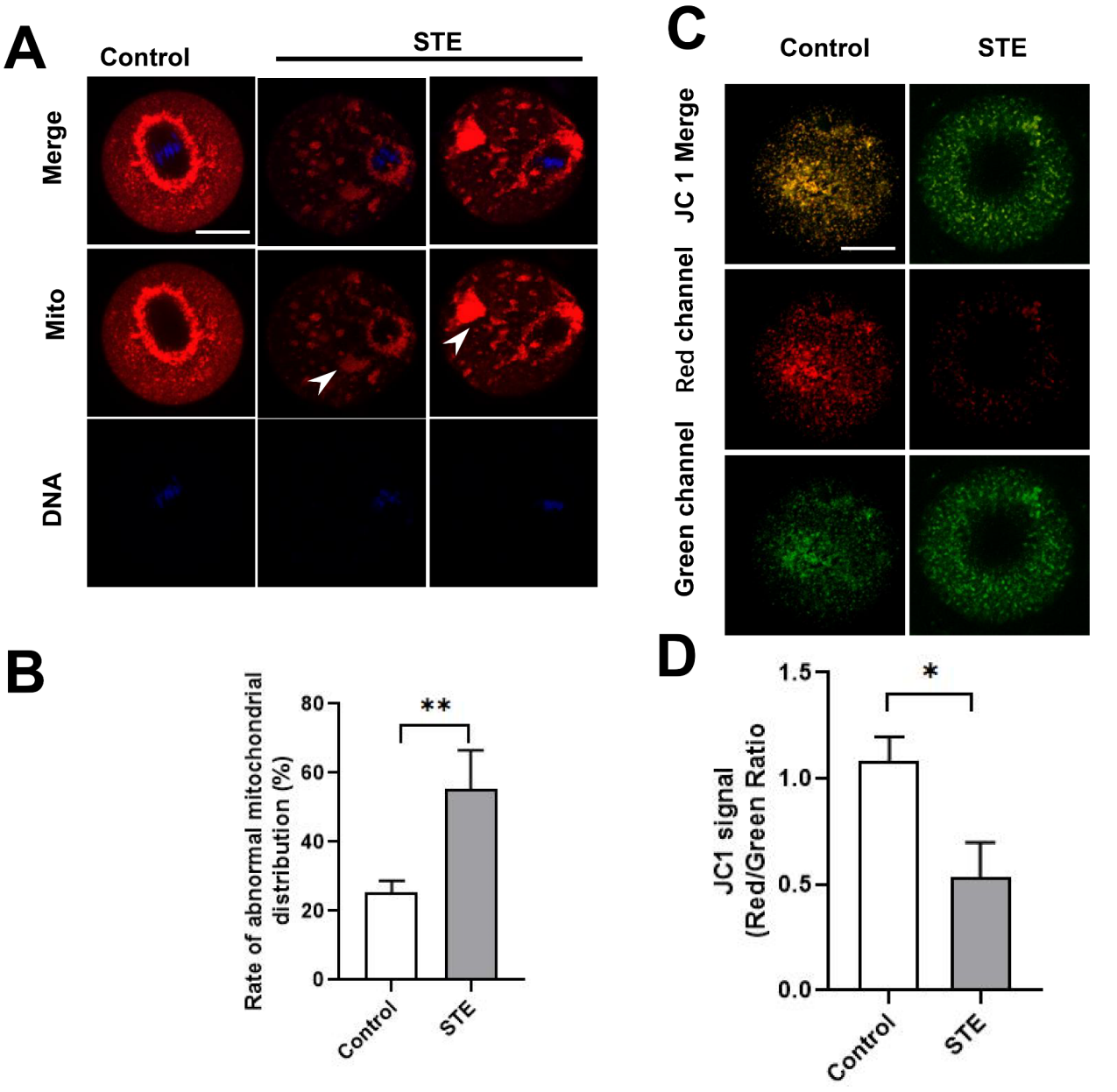


**Fig. 3** STE exposure disrupts mitochondrial redistribution and membrane potential in oocytes. Control and STE-exposed oocytes were labeled with MitoTracker Red to visualize mitochondrial localization and counterstained with Hoechst 33,342 to show meiotic stages. We evaluated mitochondrial distribution patterns using confocal microscopy. (**A**) Representative images of mitochondrial distribution patterns in MI oocytes: polarized distribution, homogeneous distribution, and clustered distribution. White arrowheads represent mitochondria distributed in clusters. (**B**) Quantification of control and STE-exposed oocytes at the MI stage with each mitochondrial distribution pattern (control group, 25.3 ± 2.87% [number of replicates = 3, number of oocytes = 51, and number of mice = 3]; STE group, 55.4 ± 9.09% [number of replicates = 3, number of oocytes = 65, and number of mice = 3]; $p < 0.01$). (**C**) Mitochondrial membrane potential in control and STE-exposed oocytes as measured using JC-1 fluorescence; the green fluorescence shows inactive mitochondria, and the red fluorescence shows active mitochondria. (**D**) Histogram depicting the JC-1 red/green fluorescence ratio in the control and STE-exposed groups (control group, 1.08 ± 0.10 [number of replicates = 3, number of oocytes = 43, and number of mice = 4]; STE group, 0.54 ± 0.14 [number of replicates = 3, number of oocytes = 51, and number of mice = 4]). Error bars indicate mean ± SD (** $p < 0.01$; scale bar, 25 μm)

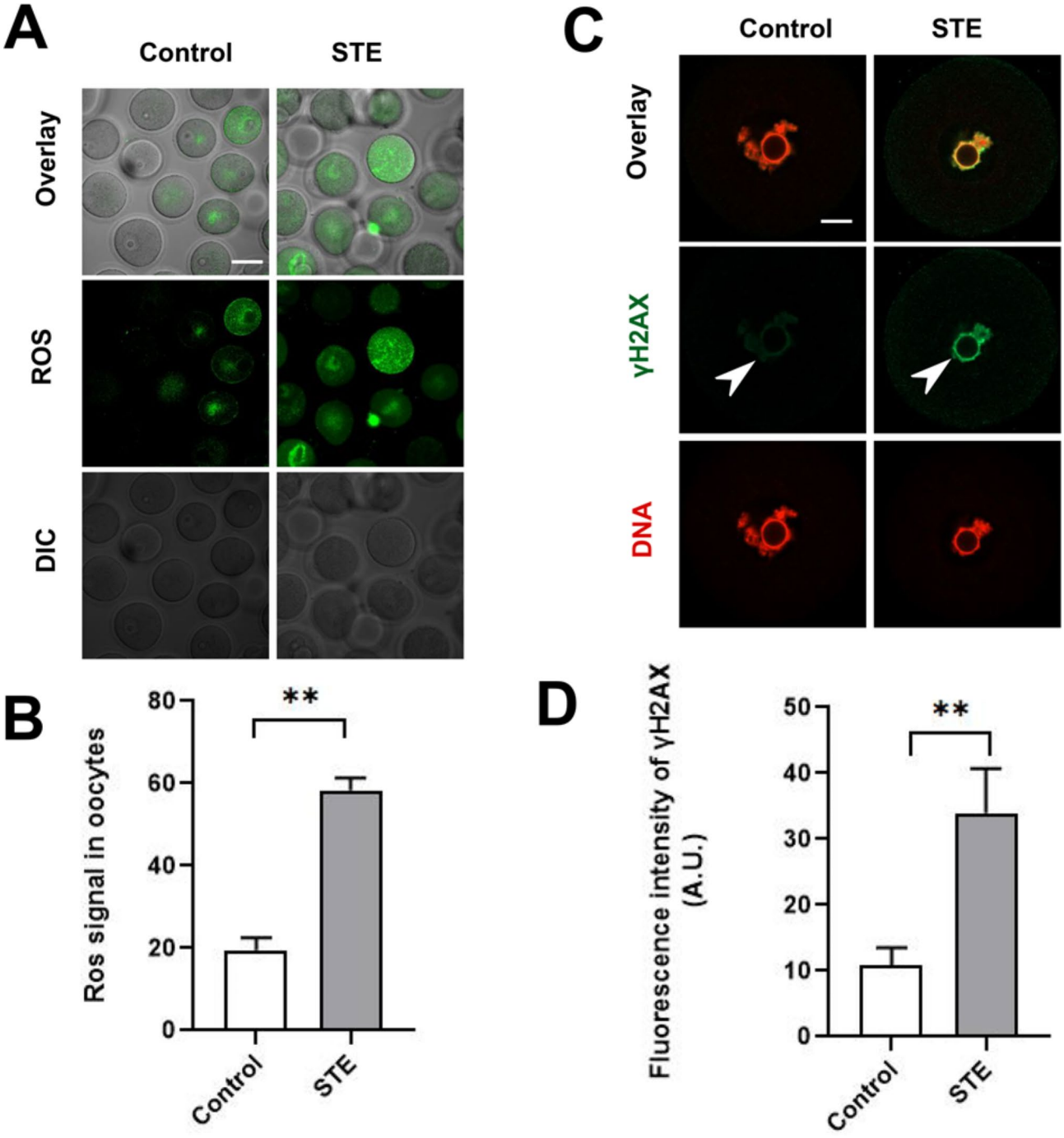


**Fig. 4** STE exposure induces an increase in oxidative stress and DNA damage in mouse oocytes. (**A**) Representative images of CMH2DCFAD fluorescence in control and STE-exposed oocytes (scale bar, 80 μm). (**B**) Quantitative analysis of fluorescence intensity in control and STE-exposed oocytes (control group, 19.5 ± 2.95 [number of replicates = 3, number of oocytes = 32, and number of mice = 3]; STE group, 58.3 ± 2.98 [number of replicates = 3, number of oocytes = 38 and number of mice = 3]; $p < 0.01$). (**C**) Representative images of DNA damage in control and STE-exposed oocytes (scale bar, 20 μm). Arrows represent aggregated γH2AX signals. (**D**) Fluorescence intensity of γH2A.X signals was quantified in control and STE-exposed oocytes (control group, 10.1 ± 1.60 [number of replicates = 3, number of oocytes = 35, and number of mice = 3]; STE group, 29.1 ± 1.93 [number of replicates = 3, number of oocytes = 41, and number of mice = 3]). Data are expressed as the mean ± SD from three independent experiments (**significantly different at $p < 0.01$)

a greater occurrence of DNA damage in oocytes (arrows) (control group, 10.1±1.60 [number of replicates=3, number of oocytes=35, and number of mice=3]; STE group, 29.1±1.93 [number of replicates=3, number of oocytes=41, and number of mice=3]; $p<0.01$) (Fig. 4C and D). Thus, these results implied that STE exposure induced the accumulation of excessive ROS to generate DNA damage, consequently producing poorer quality oocytes.

### STE exposure disrupts assembly of the spindle/chromosome in mice oocytes

To explore the reason for oocyte maturation defects in the STE-exposed oocytes, we examined spindle morphology in vitro culture for 8 h after STE treatment. Immunofluorescence data revealed that a large number of control oocytes have a regular spindle with a conventional shape and well-aligned chromosomes at the MI stage (Fig. 5A). In contradistinction, a higher incidence of spindle assembly abnormalities (arrows) and unconventional chromosomal alignments was observed in the STE-exposed oocytes (Fig. 5A), and we noted that the proportion

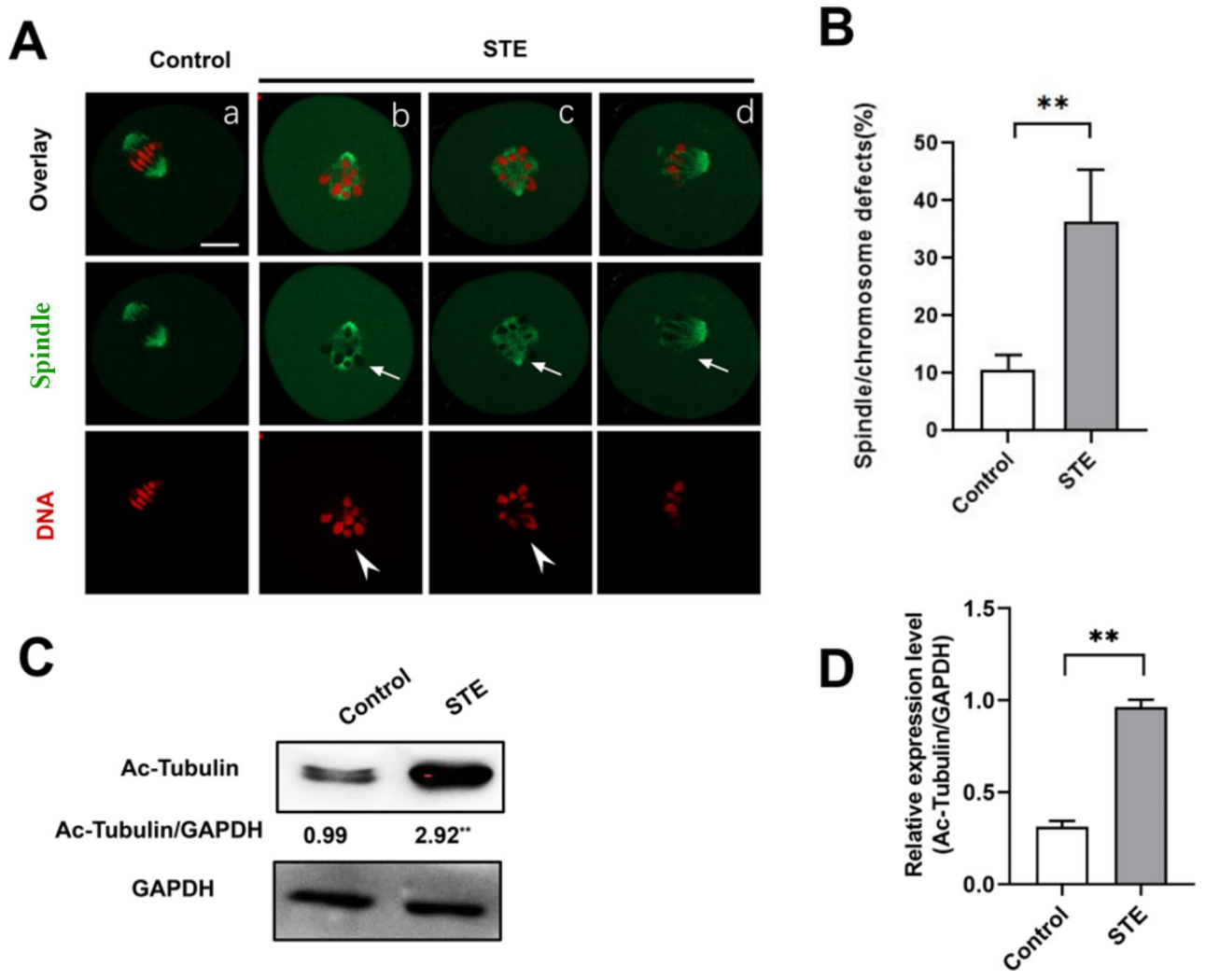


**Fig. 5** STE exposure disrupts assembly of the spindle/chromosome apparatus in mouse oocytes. (**A**) Oocytes were immunostained with anti-α-tubulin-FITC antibody to visualize spindle morphology (green) and counterstained with propidium iodide (PI) to show chromosomal alignment (red). (a) Control oocytes exhibit the characteristic barrel-shaped spindle and well-aligned chromosomes. (b-d) Three examples illustrate the disorganized spindles (arrows) and misaligned chromosomes (arrowheads), which were frequently observed in STE-exposed oocytes (scale bar, 20 μm). (**B**) The proportion of aberrant spindles and chromosome alignment were quantified in control and STE-exposed oocytes (control group, 10.5 ± 2.20% [number of replicates = 3, number of oocytes = 53, and number of mice = 3; STE group, 36.3 ± 7.43% [number of replicates = 3, number of oocytes = 57, and number of mice = 3]). (**C**) Expression of acetylated tubulin levels in control and STE-exposed oocytes. Proteins from 200 oocytes were loaded for each sample. (**D**) Relative-intensity results for AC-Tubulin protein expression in the control and STE-treated oocytes. Data are presented as mean percentage (mean ± SD) from at least three independent experiments (**significantly different at $p < 0.01$)

of STE-treated oocytes with spindle/chromosome defects was remarkably higher than in control oocytes (control group, 10.5±2.20% [number of replicates=3, number of oocytes=53, and number of mice=3]; STE group, 36.3±7.43% [number of replicates=3, number of oocytes=57, and number of mice=3]; $p<0.01$) (Fig. 5B), indicating that STE exposure induces a defective spindle/chromosome structure in mouse oocytes. We finally examined whether STE exposure affects α-tubulin acetylation levels in mouse oocytes, we found that STE treatment increases oocyte ac-tubulin levels (Fig. 5C and D).

### Exposure to STE toxin affects meiotic progression and perturbs the actin caps during mouse oocyte maturation

Next, we used phalloidin-TRITC to stain oocytes that cultured in vitro for 8 h (MI) after STE treatment and determined whether the STE-exposure affected actin polymerization. According to the Fig. 6A and B, actin caps were visible in approximately 81% and 40% of control and STE-treatment oocytes, respectively. (control group, 81.0±1.96% [number of replicates=3, number of oocytes=32, and number of mice=3]; STE group, 40.8±2.16% [number of replicates=3, number of oocytes=37, and number of mice=3]; $p<0.01$). In addition, nuclear staining and quantitative analysis revealed that the proportion of oocytes arrest in GVBD stage increased significantly after 8 h of STE treatment. (control group, 18.9±1.90% [number of replicates=3, number of oocytes=32, and number of mice=3]; STE group, 40.1±1.62% [number of replicates=3, number of oocytes=37, and number of mice=3]; $p<0.01$) (Fig. 6C). In summary, we demonstrated that STE treatment affects the development process of oocytes and perturbs the formation of actin cap.

### STE exposure induces ferroptosis and reduces pERK1/2 expression in mouse oocytes

Our RNA-seq data revealed that STE exposure induces oocyte ferroptosis process. And we observed that $Fe^{2+}$ level was increased in oocytes cultured in vitro for 8 h (MI) after STE treatment (control group, 32.3±3.86 [number of replicates=3, number of oocytes=33, and number of mice=3]; STE group, 19.0±1.63 [number of replicates=3, number of oocytes=36, and number of mice=3]; $p<0.01$) (Fig. 7A, B). While ferroptosis-related protein expression levels of GPX4 and ACSL4 were significantly upregulated (Fig. 7C-F). Next, we examined the effects of STE supplementation on GSH levels in oocytes. Figure 7G shows weak GSH fluorescence signals were generated in STE exposure oocytes (control group, 31.7±2.8 [number of replicates=3, number of oocytes=35, and number of mice=3]; STE group, 16.0±2.94 [number of replicates=3, number of oocytes=33, and number of mice=3]; $p<0.01$). Thus, these data suggested that STE exposure induced ferroptosis, consequently resulting in poorer quality oocytes.

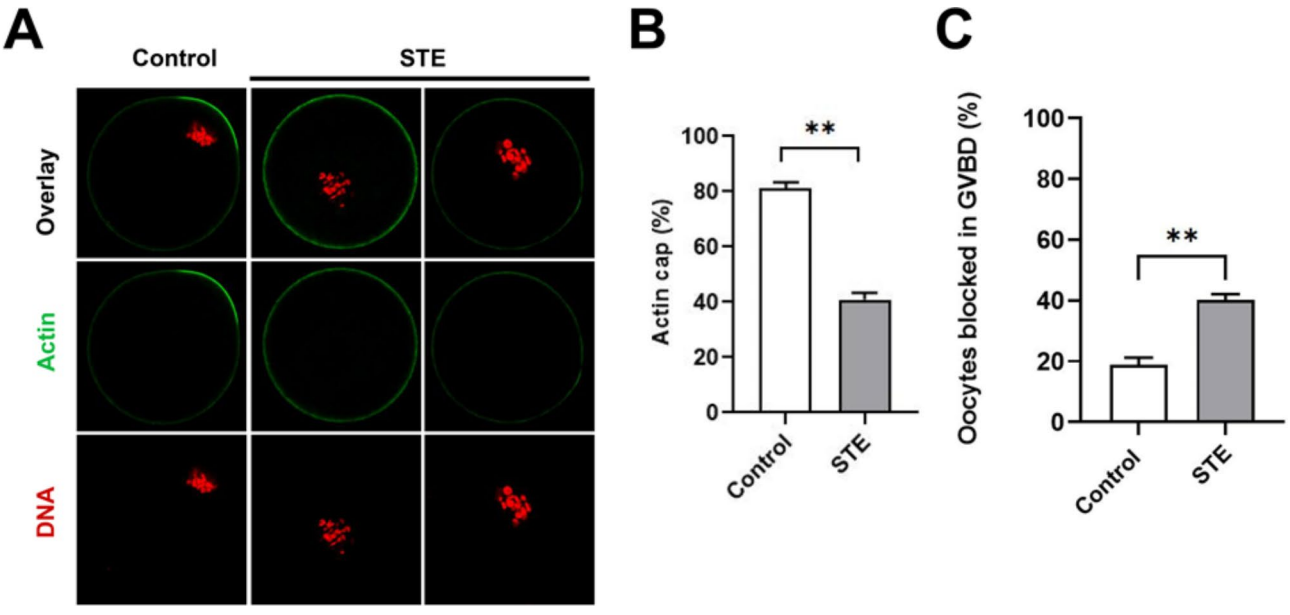


**Fig. 6** Exposure to STE toxin perturbs the actin cytoskeleton during mouse oocyte meiosis. (**A**) Representative images of actin filaments on the plasma membrane in control and STE-exposed oocytes (scale bar, 20 μm). (**B**) Quantification of control and STE-exposure oocytes with formation a normal actin cap (control group, 81.0 ± 1.96% [$n=32$]; STE group, 40.8 ± 2.16% [$n=37$]; $p<0.01$). (**C**) Percentage of GVBD-arrested oocytes after STE exposure (control group, 18.9 ± 1.90% [number of replicates = 3, number of oocytes = 32, and number of mice = 3]; STE group, 40.1 ± 1.62 [number of replicates = 3, number of oocytes = 37, and number of mice = 3]; $p<0.01$). Data are presented as mean percentage (mean ± SD) from at least three independent experiments (**significantly different at $p<0.01$)

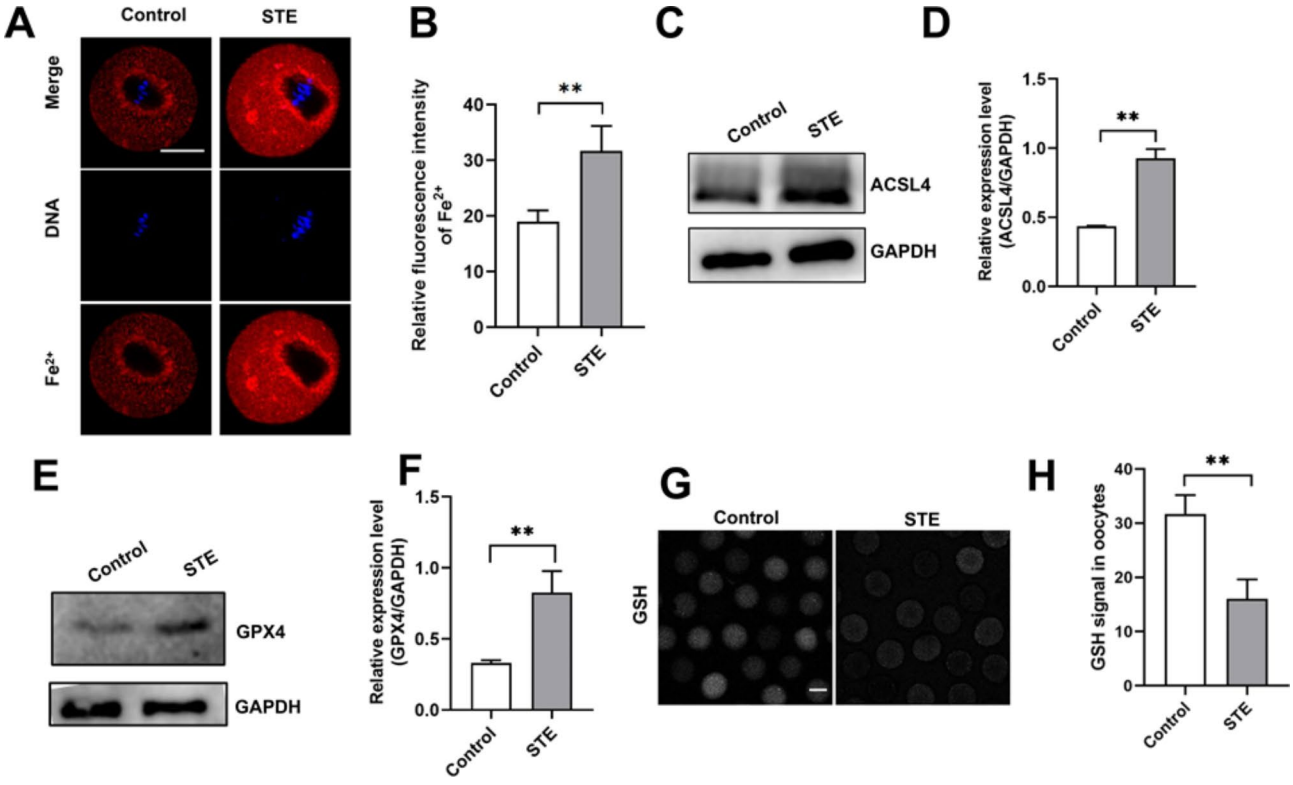


**Fig. 7** STE exposure induces ferroptosis and reduces pERK1/2 expression in mouse oocytes. (**A**) Representative images of $Fe^{2+}$ fluorescence in control and STE-exposed oocytes (scale bar, 20 μm). (**B**) Quantitative analysis of $Fe^{2+}$ fluorescence intensity in control and STE-exposed oocytes (control group, control group, 32.3 ± 3.86 [number of replicates = 3, number of oocytes = 33, and number of mice = 3]; STE group, 19.0 ± 1.63 [number of replicates = 3, number of oocytes = 36, and number of mice = 3]). (**C**) Expression of GPX4 levels in control and STE-exposed oocytes. Proteins from 200 oocytes were loaded for each sample. (**D**) Relative-intensity results for GPX4 protein expression in the control and STE-treated oocytes. (**E**) Expression of ACSL4 levels in control and STE-exposed oocytes. Proteins from 200 oocytes were loaded for each sample. (**F**) Relative-intensity results for ACSL4 protein expression in the control and STE-exposed oocytes. (**G**) Representative images of GSH fluorescence in control and STE-exposed oocytes (scale bar, 80 μm). (**H**) Quantitative analysis of GSH fluorescence intensity in control and STE-exposed oocytes (control group, 31.7 ± 2.87 [number of replicates = 3, number of oocytes = 35, and number of mice = 3]; STE group, 16.0 ± 2.94 [number of replicates = 3, number of oocytes = 33, and number of mice = 3]). Experiments were repeated three times, and the results are presented as mean ± SD (*significantly different at $p < 0.05$ and **significantly different at $p < 0.01$)

### STE exposure inhibits RAF1 activity and induced oocyte asymmetric division defects

As a serine/threonine protein kinase, RAF1 activity is required for progesterone-induced oocyte maturation [25]. According to the results from RNA-sequencing, we found that STE exposure significantly reduced *Raf1* mRNA levels (Supplementary Material 1). When RAF1 protein expression was then assessed by western blotting in oocytes exposed to STE for 8 h in vitro, we found it to be significantly reduced (Fig. 8A and B). In addition, we noted that STE treatment significantly reduced the phosphorylation of ERK1/2 (Fig. 8C-E). Considering the important role of RAF1 during oocyte development, mouse oocytes were treated with a RAF1 specific inhibitor (10 μM), WB results revealed that RAF1 protein expression significantly reduced after RAF1 inhibitor treatment for 8 h in vitro (Fig. 8F and G). After 14 h in vitro culture, we observed the first polar body extrusion rate of oocytes in the control and RAF1-inhibited groups, and we noted that when the activity of RAF1 was inhibited, the asymmetric defects (large polar body) of oocytes significantly increased (Fig. 8H and I). Collectively, our results demonstrated that the inhibition of RAF1 activity by STE is one of the factors responsible for the defect in oocyte asymmetric division.

## Discussion

Toxic chemicals can disrupt oocyte growth and embryonic development [26]. As a mycotoxin, STE is widely present in human environments, including foods, feeds, and indoor dust [27]. The STE is generally recognized as a possible carcinogen, mutagen, and teratogen [28]. Extensive evidence demonstrated that exposure to STE induced adverse effects on organisms and in particular its reproductive toxicity has been attracted public concern [29]. In the present study, we focused on the effects of STE exposure on mouse oocyte maturation and our findings revealed that STE exposure reduced the emission of the first polar body as well as disrupted the asymmetric division in mouse oocytes.

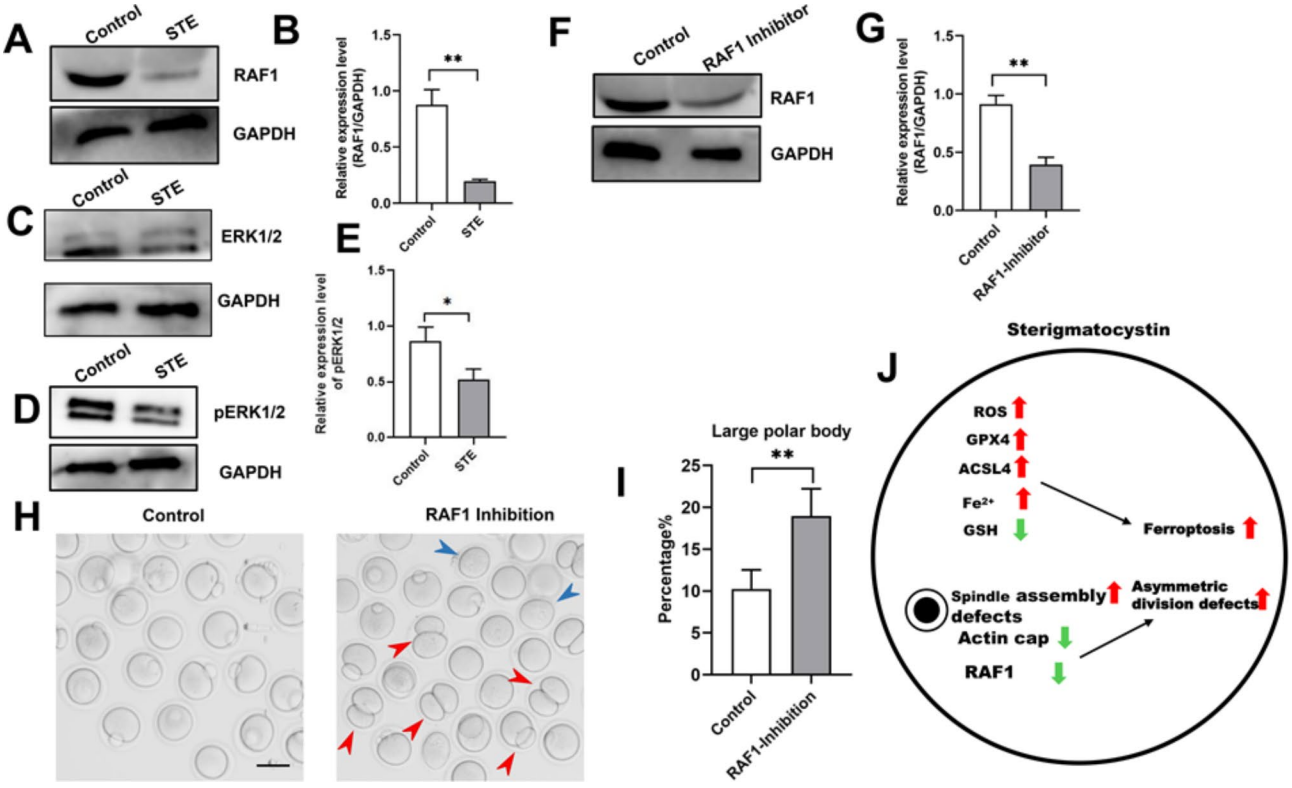


**Fig. 8** STE exposure inhibits RAF1 activity and induced oocyte asymmetric division defects. (**A**) Expression of RAF1 levels in control and STE-exposed oocytes. Proteins from 100 oocytes were loaded for each sample. (**B**) Relative-intensity results for RAF1 protein expression in the control and STE-treated oocytes. (**C**) Expression of ERK1/2 levels in control and STE-exposed oocytes. Proteins from 100 oocytes were loaded for each sample. (**D**) Expression of pERK1/2 levels in control and STE-exposed oocytes. Proteins from 100 oocytes were loaded for each sample. (**E**) Relative-intensity results for pERK1/2 protein expression in the control and STE-exposed oocytes. (**F**) Expression of RAF1 levels in control and RAF1-Inhibitor oocytes. Proteins from 100 oocytes were loaded for each sample. (**G**) Relative-intensity results for RAF1 protein expression in the control and RAF1-Inhibitor oocytes. (**H**) Representative images of oocytes from control and RAF1-Inhibitor groups. Red arrowheads denote oocytes with apparent symmetrical division and blue arrowheads indicate oocytes that fail to extrude polar bodies (scale bar, 80 μm). (**I**) The percentage of oocytes with large polar bodies after STE-treated. And the proportion of large polar body was (10.3 ± 1.86% [number of replicates = 3, number of oocytes = 105, and number of mice = 6], 19.0 ± 2.67% [number of replicates = 3, number of oocytes = 121, and number of mice = 6], $p < 0.01$) in control and RAF1 Inhibition groups. (**J**) Proposed model for the role of STE in oocyte maturation. STE exposure caused abnormal expression of GPX4 and ACSL4, which induced ferroptosis in oocytes. In addition, STE exposure inhibited RAF1 activity, which is one of the reasons for the defects in STE-induced asymmetric division in mice oocytes. Experiments were repeated three times, and the results are presented as mean ± SD (*significantly different at $p < 0.05$ and **significantly different at $p < 0.01$)

Our results showed that STE exposure significantly decreased the developmental capacity of mouse oocytes, showing by a reduction in the rate of the first polar body extrusion and asymmetric division defects in a dose dependent manner. A key indicator of oocyte maturation is the extrusion of the first polar body (Pb1) [30]. This may also suggest that STE exposure could cause the decline of oocyte quality. Oocyte maturation is a complex process. Mouse oocytes reach maturity within 14 h during in vitro maturation, but it takes much longer in vivo [31]. In our study, we examined the impact of exposure dose and duration on the maturation of oocytes, finding that a higher concentration of STE (100 μM, 32.42 ng/μL) inhibited the maturation of most oocytes while enabling a minority to reach maturity. Furthermore, intrabdominal injection of STE has been shown to reduce the growth rate of chicks [32]. The levels of STE were detected in human breast milk (1.2 ng/L) [33] and plasma (1.0–30.0 ng/μL) [34]. Our results confirmed that exposure to 100 μM (32.42 ng/μL) caused meiosis failure in mouse oocytes, this concentration is slightly higher than that found in human plasma. In addition, our results also demonstrated that STE could induce oocyte meiosis abnormalities even at 25 μM (8.1 ng/μL). Although the concentration of STE in mammalian and human follicular fluid has not been reported, our results show that STE can interfere with the meiosis process of mouse oocytes even at low levels of exposure.

Studies have demonstrated that STE could induce oxidative stress, mitochondrial dysfunction, apoptosis, and cell cycle arrest [12]. The status of mitochondria in the experimental mouse oocytes became our first object of assessment. The distribution pattern of mitochondria has been correlated with the quality and developmental

potential of mammalian oocytes and embryos in scientific literature [35, 36]. In this study, we focused on the mitochondrial distribution patterns of oocytes in the control and STE treated oocytes cultured in vitro for 8 h. The mitochondrial distribution pattern of most oocytes in the control group showed polarized distribution, however, oocytes in the STE-treated group showed a high proportion of clustered distribution. In addition, we noted that STE-exposed oocytes exhibited a markedly reduced mitochondrial membrane potential in mouse oocytes, diminished mitochondrial membrane potential indicates mitochondrial dysfunction [37]. It was previously noted that STE administration generates free radicals, induces lipid peroxidation and changes in cellular antioxidant status [38]. We observed that ROS levels were dramatically augmented with STE exposure, suggesting mitochondrial dysfunction. Increased production of reactive oxygen species (ROS) by mitochondria has deleterious effects on various cellular components such as DNA, RNA, proteins, and lipids, leading to disruptions in key biological processes including cellular metabolism, apoptosis, and senescence [39]. The MAPK signaling pathway, which includes p38 MAPK, extracellular signal kinase (ERKs), and c-Jun-terminal kinases (c-JNKs) [40]. The ERK signaling pathway is fundamentally known as a regulator of cell proliferation, and is downregulated by oxidative stress [41]. ERK1/2-depleted oocytes had poorly-assembled metaphase II (MII) spindles [42]. Our results also showed that STE treatment reduced phosphorylation of ERK1/2 in oocytes. Inhibition of the ERK activation increased mitochondrial ROS levels and the cell death rate of T-ALL cells [43], our RNA-seq results showed that STE exposure decreased *Dusp1* gene expression in mouse oocytes (Supplementary material 1). It has been reported that inhibition of DUSP1 can induce apoptosis in human MGC803 and MKN45 gastric cancer (GC) cell lines by inactivating MAPK [44]. However, *Dusp1*-Knockdown could activate the ERKs in HEK293T cell [45], which may be related to the differences in the use of cell lines. Inhibition of DUSP1 in cumulus cells caused abnormal cell cycle progression [46] and DUSP1 might be a potential biomarker to diagnose oocyte quality [47] .

Moreover, ROS constituted an important factor causing DNA lesions in cells [48]. The accumulation of γH2AX signal in STE-exposed oocytes indicates the STE can induce oocyte DNA damages. When DNA damage occurs in cells, it triggers cell cycle arrest and DNA repair responses [49], which to some extent explains why STE causes oocyte development arrest. Mitochondrial function and redox state are important for the proper assembly of meiotic structures during oocyte meiosis, and increased oxidative stress is tied to spindle disorganization and chromosomal misalignment in oocytes [50]. Female reproductive disorders have been linked to ferroptosis [51]. During ferroptosis, granulosa cells, oocytes and embryos can be damaged [52]. Through its ability to scavenge lipid peroxides, GPX4 is one of the inhibitors of ferroptosis [53], and *Gpx4* knockout causes cell death [54]. In our research, RNA sequencing results showed that *Acsl4* mRNA expression was downregulated in STE-treated oocytes, however, ACSL4 protein was upregulated. Previous research has indicated that while protein is more closely linked to the target of natural selection, gene expression is commonly quantified through mRNA levels. However, the assumption that mRNA levels accurately reflect protein levels has been challenged by various studies, suggesting that mRNA levels do not consistently predict protein levels [55]. In this study, we cultured oocytes in vitro for 8 h after STE treatment for RNA-Seq and Western blot. When oocytes were treated with STE, the intracellular ferroptosis process was activated, leading to an increase in ACSL4 protein expression. Since cells need a stable environment, they become stressed when protein levels rise. To maintain homeostasis, cells will inevitably reduce gene transcription [56].

In addition to its role in polyunsaturated fatty acid (PUFA) biosynthesis, ACSL4 promotes the accumulation of lipid peroxidation products [57]. Investigators have shown that STE caused lipid peroxidation [58] and that STE treatment attenuated cell proliferation and augmented apoptosis in SH-SY5Y cells [59]. It is believed that microtubules (MTs) play a significant role in organelle transport and positioning, regulation cell shape, and motility [60]. Acetylation of α-tubulin on lysine 40 is one of the major microtubular posttranslational modifications [61], and α-tubulin acetylation serves as a marker for the presence of stable MTs [62]. The function(s) of acetylated MTs during meiosis remain unknown, although acetylated MTs have been detected in mouse oocytes. Reduced tubulin acetylation has been found to decrease microtubule stability, but high tubulin acetylation did not maintain microtubule stability [63]. During mouse oocyte meiosis, altered tubulin acetylation causes spindle assembly defects and chromosome misalignment [64]. The elevated acetylation of tubulin by HDAC3 damages the stability of microtubules during oocyte maturation [65], nevertheless, reduced tubulin acetylation by RASSF1A impairs the stability of microtubules as well [66]. There is still much to learn about how tubulin acetylation affects microtubule stability.

RAF1 is a serine/threonine protein kinase that plays an essential role in cell proliferation [67]. The *Raf1*$^{-/-}$ mice die by embryonic day e12.5 [68]. The interaction between RAF1 and cytoskeletal actin is critical for its redistribution and proliferation in the airways [67]. In our research, we noted that RAF1 inhibition affected RAF1 expression, this may be because the inhibition of RAF1

interferes with meiotic process of oocytes, it means that the oocytes obtained at 8 h of RAF1 inhibitor treatment were at different developmental stages. In mouse granulosa cells, RAF1 stimulates ERK phosphorylation to synthesis and secrete estradiol [69]. RAF1 kinase activity is required for Xenopus oocyte maturation [25]. Our data revealed that STE exposure inhibits the kinase activity of RAF1, and oocytes with inhibitors of RAF1 kinase can lead to asymmetric division defects in oocytes. This can at least partially explain the development abnormalities of oocytes caused by STE exposure.

Collectively, our results provided evidence that STE exposure induced mitochondrial dysfunction, DNA damage, and ferroptosis in mouse oocytes. In addition, STE exposure inhibited RAF1 activity, which is one of the reasons asymmetric division defects (Fig. 8J).

## Materials and methods

All chemicals and culture media were purchased from Sigma (St. Louis, MO, USA) unless stated otherwise.

### Mice

The mice used in this study were purchased from Beijing Sibefu Biotechnology Co., Ltd, and 6–8-week-old ICR female mice were used in all experiments. All experimental animal protocols were performed following relevant ethical guidelines and regulations and approved by the First Affiliated Hospital of Anhui Medical University.

### Antibodies and chemicals

Mouse monoclonal anti-α-tubulin-FITC antibody (Cat#: F2168), propidium iodide (Cat#: P4170), phalloidin-TRITC (Cat#: P1951), and RAF1 specific inhibitor (Cat#: 220904-83-6) were purchased from Sigma (St. Louis, MO, USA); mouse polyclonal anti-GPX4 (Cat#: 67763-1-Ig); rabbit polyclonal anti-ACSL4 (Cat#: 22401-1-AP), mouse monoclonal anti-RAF1 (Cat#: 66592-1-Ig), rabbit polyclonal anti-pERK1/2 (CAT#:28733-1-AP), and mouse monoclonal anti-GAPDH antibody (Cat#: 60004–1 g) were bought from Proteintech (Wuhan, China); mouse monoclonal anti-acetyl-tubulin (Lys-40) (Cat#: sc-23950) antibody were obtained from Santa Cruz Biotechnology, rabbit polyclonal anti-ERK1/2 (Cat#: abs130092) was obtained from Absin (Shanghai, China). We obtained HRP-conjugated rabbit (Cat#: 7074 S) and mouse (Cat#: 7076 S) secondary antibodies from Cell Signaling Technology (Danvers, MA, USA).

### Oocyte collection and culture

To obtain fully grown GV oocytes, 6–8-week-old ICR mice were superovulated with 10 IU of pregnant mare serum gonadotropin (PMSG; SANSHENG BIOLOGICAL TECHNOLOGY, Ningbo, China) by intraperitoneal injection; 48 h later, GV oocytes were harvested from the mouse ovaries and placed in M2 (Sigma, St. Louis, MO, USA; Cat#: M7167) medium. Oocytes were subsequently cultured in mini-drops of M16 (Sigma, St. Louis, MO, USA; Cat#: MR-016) medium covered with mineral oil (Sigma, St. Louis, MO, USA; Cat#: M8410) at 37 °C in an atmosphere of 5% $CO_2$ in compressed air and high humidity.

### STE treatment

STE (CAT#: S102406, *Aladdin*, Shanghai, China) was dissolved in dimethyl sulfoxide (DMSO) after centrifugation and was diluted in M16 medium to produce final concentrations of 25, 50, 100 and 200 μM. The control oocytes were grown in M16 medium with the same concentration of DMSO (0.05%). The final DMSO concentration was 0.05% in each experiment group. After culture 3 h and 14 h, the germinal vesicle breakdown (GVBD) and metaphase II (MII) oocytes were used for the subsequent experiments.

### RNA – sequencing (RNA-seq) and analysis

In both control and STE exposure groups, total RNA was extracted oocytes after 8 h of culture. We collected 40 oocytes for each group for disposal by the Beijing Allawe Gene Technology Co. Ltd. The total RNA was first extracted using the TRIzol method (Invirtrogen, CA, USA) and treated with RNase-free DNase I (Takara, Kusatsu, Japan). RNA degradation and contamination were monitored on 1% agarose gels. RNA was quantified using Agilent 2100 Bioanalyzer (Agilent Technologies, CA, USA), the quality and integrity were assessed by NanoDrop spectrophometer (Thermo Scientific, DE, USA). RNA samples with concentrations higher than 200 ng/μL were considered eligible. A total of 1.5 μg of RNA per sample was utilized for RNA sample preparations. Sequencing libraries were constructed using the NEBNext® Ultra™ RNA Library Prep Kit for Illumina® (NEB, USA) in accordance with the manufacturer's instructions. To isolate cDNA fragments ranging from 200 to 250 bp in length, the library fragments were purified using the AMPure XP system (Beckman Coulter, Beverly, USA). The library preparations were sequenced on an Illumina Novaseq 6000 platform by the Beijing Allwegene Technology Company Limited (Beijing, China), resulting in the generation of paired-end 150 bp reads.

Gene expression levels were quantified using fragments per kilobase of transcript per million fragments mapped (FPKM). Differential expression analysis between two groups was conducted utilizing the DESeq R package (version 1.10.1). To account for multiple testing, the resulting P values were adjusted using the Benjamini and Hochberg method to control the false discovery rate. Genes with an adjusted P-value$<$0.05 as determined by DESeq were classified as differentially expressed.

The GOseq R packages were utilized to conduct Gene Ontology (GO) enrichment analysis on the differentially expressed genes (DEGs), employing the Wallenius non-central hyper-geometric distribution to account for gene length bias.

KEGG serves as a database resource for comprehending the overarching functions and utilities of biological systems, ranging from cellular to ecosystem levels, by leveraging molecular-level data, particularly from large-scale molecular datasets produced through genome sequencing and other high-throughput experimental methodologies (http://www.genome.jp/kegg/). We used KOBAS software to test the statistical enrichment of differential expression genes in KEGG pathways.

#### Immunofluorescence microscopy

Oocytes were first fixed in 4% paraformaldehyde for 30 min at 4℃ and then permeabilized with 0.5% Triton X-100 for 20 min. Oocyte protein binding sites were then blocked in 1% BSA-supplemented phosphate-buffered saline (PBS) for 1 h and stained with different first antibodies (1:250 for γH2AX) at 4 °C overnight. After extensive washing, the samples were then stained with rabbit secondary antibodies (CST, Cat#: 7074 S, 1:300) at 37 °C for 1 h. For spindle staining, oocytes were immunolabeled with anti- α- tubulin- FITC antibody (Sigma, Cat#: F2168, 1:300) to visualize the spindle. Oocytes were stained with PI (10 mg/mL in PBS) for 10 min at room temperature and ultimately examined with a laser-scanning confocal microscope (Zeiss LSM 800 META; Jena, Germany). To assess mitochondrial staining in oocytes, the cells were incubated in M2 medium supplemented with 200 nM MitoTraker Red (Invitrogen, Cat#: M7152) for 30 min at 37℃. Subsequently, the oocytes underwent three washes with M2 medium before being examined using a confocal laser scanning microscope. Evaluation of mitochondrial membrane potential (MMP) was conducted by culturing oocytes in M2 medium containing 2 μM JC-1 for 30 min at 37℃. The mitochondrial membrane potential was determined by quantifying the ratio of red fluorescence, indicative of activated mitochondria (J-aggregates), to green fluorescence, indicative of less activated mitochondria (J-monomers). For F-actin staining, the samples were fixed with 4% paraformaldehyde for 5 min and then blocked with 1% BSA for 1 h. Following a 1 h incubation period with FITC-conjugated phalloidin (5 μg/mL in PBS), the DNA was subsequently counterstained with PI for 10 min. Subsequently, the oocytes were washed three times and co-stained with propidium iodide (10 mg/mL in PBS) for 10 min and then mounted on glass slides.

#### Assays of intracellular ROS and GSH levels

Denuded oocytes were added to medium that contained 5 uM 2',7'-dichlorofluorescin diacetate (2',7'-DCFHDA) or 10 μM Cell Tracker Blue to measure ROS or GSH at 37 °C for 30 min. After three washes with M2, the oocytes were placed on glass slides for further detection under a laser scanning confocal microscope (LSM 800, Zeiss, Germany). The fluorescence of each oocyte was analyzed by Zeiss software (ZEISS, Germany).

#### Ferrous ion staining

Consistent with the oocyte developmental stage of the previous RNA sequencing, intracellular $Fe^{2+}$ levels were examined at the 8 h of the IVM period. The oocytes in each group were thoroughly washed in prewarmed M2 medium and assessed using the 1 μM fluorescent probe Ferro Orange (Dojindo, Cat#: F374) for 30 min. After three washes, the oocytes were placed on confocal dishes for further detection under a laser scanning confocal microscope (LSM 800, Zeiss, Germany).

#### Analysis of fluorescence intensity

Oocytes in the control and experimental groups were mounted on the same glass slide, and the same previous scan settings were used for sample scanning with a Zeiss LSM 800 META confocal system. The same immunostaining procedure was performed on control and STE-exposed oocytes to measure fluorescence intensity and the same parameters were used as with confocal microscopes. Image J software was utilized to delineate a region of interest (ROI) and calculate the average fluorescence intensity per unit area within the ROI. The resulting average values were then compared between the control and STE groups to assess differences in fluorescence intensity.

#### Western blot analysis

A total of 200 mouse oocytes in each group were collected and lysed in Laemmli sample buffer (95% Laemmli sample buffer and 5% β-mercaptoethanoll). The samples were first boiled at 100 °C for 10 min, and then subjected to SDS-polyacrylamide gel electrophoresis (PAGE) using 10% gels in Tris/Glycine/SDS Running Buffer (Epizyme, China, Cat: # PS105S). After electrophoretic separation, proteins were transferred onto polyvinylidene fluoride membranes (Millipore, Billerica, MA, USA); membranes were blocked with Tris-buffered saline (TBS) that contained 0.1% (w/w) Tween 20 (TBST) and 5% nonfat dry milk at 37 °C for at least 1 h. After a brief wash in TBST, the membranes were incubated with a mouse monoclonal anti-GPX4 antibody (1:1000), rabbit monoclonal anti-ACSL4 antibody (1:1000), mouse monoclonal anti-RAF1 antibody (1:2000), mouse monoclonal anti-acetyl-tubulin (Lys-40) (1:200), rabbit polyclonal anti-pERK1/2 (1:2000), rabbit polyclonal anti-ERK1/2 (1:2000) and a mouse

monoclonal anti-GAPDH antibody (1:5000) at 4 °C overnight. After washing three times in TBST (10 min each), membranes were incubated for 1 h with secondary anti-rabbit or anti-mouse HRP-conjugated antibodies (1:5000) in 5% nonfat dry milk in TBST. The membranes were then exposed to an enhanced chemiluminescence reagent (Epizyme, Shanghai, China). For quantitation of Western blot band intensity, densitometric analysis was performed using Image J software and normalized to either the levels of GAPDH.

### Statistical analysis

We expressed all percentages or values from at least three independent replicates as means ± SD. The normal distribution of the data was performed using Kolmogorov-Smirnov in SPSS 20.0 software. Unpaired, two-tailed Student's *t* tests were applied to assess differences between two groups, and comparisons among more than two groups were analyzed with a one-way ANOVA and Tukey's multiple-comparison test using Prism GraphPad 8. A $p$ value of $<0.05$ was considered to be statistically significant.

#### Abbreviations

| | |
|---|---|
| STE | Sterigmatocystin |
| GPX4 | Glutathione Peroxidase 4 |
| ACSL4 | Acyl-CoA Synthetase Long Chain Family Member 4 |
| PB1 | First polar body |
| IVM | In vitro maturation |

## Supplementary Information

The online version contains supplementary material available at https://doi.org/10.1186/s13048-024-01499-w.

Supplementary Material 1

Supplementary Material 2

#### Acknowledgements

We thank LetPub (www.letpub.com) for its linguistic assistance during the preparation of this manuscript.

#### Author contributions

Shiwei Wang, XuanWu, Min Li, Juan Zeng provided key intellectual input in the conception and design of these studies. Shiwei Wang and XuanWu wrote the manuscript. Juan Yang, Yuwan Peng, Min Li, Fulu Miao, Juan Zeng performed all experiments. Juan Yang, Yuwan Peng, Min Li, Fulu Miao, Juan Zeng contributed to the writing of the manuscript. All authors reviewed the manuscript.

#### Funding

This study was supported by the National Natural Science Youth Foundation of China (82301864) and Scientific Research Platform Base Construction Foundation of Anhui Medical University (2023xkjT053).

#### Data availability

All raw sequences were deposited in the NCBI Sequence Read Archive under accession numbers SRP484316. Further data requests and more information can be obtained by contacting the corresponding author Juan Zeng (juanzeng2023@163.com).

## Declarations

#### Ethics approval and consent to participate

Experiments were approved by the First Affiliated Hospital of Anhui Medical University Care and Use Committee and conducted in accordance with the guiding principles of the institution.

#### Competing interests

The authors declare no competing interests.

Received: 28 March 2024 / Accepted: 14 August 2024
Published online: 28 August 2024

#### References

1. Shen X, Liu X, Zhu P, Zhang Y, Wang J, Wang Y, Wang W, Liu J, Li N, Liu F. Proteomic analysis of human follicular fluid associated with successful in vitro fertilization. Reprod Biol Endocrinol. 2017;15:58.
2. Coticchio G, Dal Canto M, Mignini Renzini M, Guglielmo MC, Brambillasca F, Turchi D, Novara PV, Fadini R. Oocyte maturation: gamete-somatic cells interactions, meiotic resumption, cytoskeletal dynamics and cytoplasmic reorganization. Hum Reprod Update. 2015;21:427–54.
3. Wang F, Zhang L, Duan X, Zhang GL, Wang ZB, Wang Q, Xiong B, Sun SC. RhoA-mediated FMNL1 regulates GM130 for actin assembly and phosphorylates MAPK for spindle formation in mouse oocyte meiosis. Cell Cycle. 2015;14:2835–43.
4. Yin S, Sun QY. FMNL1, a key regulator for asymmetric cell division. Cell Cycle. 2015;14:2879–80.
5. Zhang Z, Li B, Fu J, Li R, Diao F, Li C, Chen B, Du J, Zhou Z, Mu J, et al. Bi-allelic missense pathogenic variants in TRIP13 cause female infertility characterized by oocyte maturation arrest. Am J Hum Genet. 2020;107:15–23.
6. Li J, Qian WP, Sun QY. Cyclins regulating oocyte meiotic cell cycle progressiondagger. Biol Reprod. 2019;101:878–81.
7. Duan X, Li Y, Yi K, Guo F, Wang H, Wu PH, Yang J, Mair DB, Morales EA, Kalab P, et al. Dynamic organelle distribution initiates actin-based spindle migration in mouse oocytes. Nat Commun. 2020;11:277.
8. Gilchrist RB, Luciano AM, Richani D, Zeng HT, Wang X, Vos MD, Sugimura S, Smitz J, Richard FJ, Thompson JG. Oocyte maturation and quality: role of cyclic nucleotides. Reproduction. 2016;152:R143–157.
9. Wang Y, Xing CH, Zhang HL, Pan ZN, Sun SC. Exposure to nivalenol declines mouse oocyte quality via inducing oxidative stress-related apoptosis and DNA damagedagger. Biol Reprod. 2021;105:1474–83.
10. Wagacha JM, Muthomi JW. Mycotoxin problem in Africa: current status, implications to food safety and health and possible management strategies. Int J Food Microbiol. 2008;124:1–12.
11. Fliszar-Nyul E, Faisal Z, Skaper R, Lemli B, Bayartsetseg B, Hetenyi C, Gombos P, Szabo A, Poor M. Interaction of the emerging mycotoxins beauvericin, cyclopiazonic acid, and sterigmatocystin with human serum albumin. Biomolecules 2022, 12.
12. Zingales V, Fernandez-Franzon M, Ruiz MJ. Sterigmatocystin: occurrence, toxicity and molecular mechanisms of action - A review. Food Chem Toxicol. 2020;146:111802.
13. Diaz Nieto CH, Granero AM, Zon MA, Fernandez H. Sterigmatocystin: a mycotoxin to be seriously considered. Food Chem Toxicol. 2018;118:460–70.
14. Vesonder RF, Horn BW. Sterigmatocystin in dairy cattle feed contaminated with Aspergillus Versicolor. Appl Environ Microbiol. 1985;49:234–5.
15. Fujii K, Kurata H, Odashima S, Hatsuda Y. Tumor induction by a single subcutaneous injection of sterigmatocystin in newborn mice. Cancer Res. 1976;36:1615–8.
16. Purchase IF, Van der Watt JJ. Carcinogenicity of sterigmatocystin to rat skin. Toxicol Appl Pharmacol. 1973;26:274–81.
17. Fincham JE, van Rensburg SJ, Kriek NP. Squamous cell carcinoma in an African green monkey. Vet Pathol. 1982;19:450–3.
18. Csenki Z, Risa A, Sarkany D, Garai E, Bata-Vidacs I, Baka E, Szekeres A, Varga M, Acs A, Griffitts J et al. Comparison evaluation of the biological effects of Sterigmatocystin and aflatoxin B1 utilizing sos-chromotest and a novel zebrafish (Danio rerio) embryo microinjection method. Toxins (Basel) 2022, 14.
19. Dubravka R, Daniela J, Andrea HT, Domagoj K, Nevenka K, Lada R, Davor Z, Maja P, Maja SK. Sterigmatocystin moderately induces oxidative stress in male Wistar rats after short-term oral treatment. Mycotoxin Res. 2020;36:181–91.

20. Zingales V, Sirerol-Piquer MS, Fernandez-Franzon M, Ruiz MJ. Role of quercetin on sterigmatocystin-induced oxidative stress-mediated toxicity. Food Chem Toxicol. 2021;156:112498.
21. Gao W, Jiang L, Ge L, Chen M, Geng C, Yang G, Li Q, Ji F, Yan Q, Zou Y, et al. Sterigmatocystin-induced oxidative DNA damage in human liver-derived cell line through lysosomal damage. Toxicol Vitro. 2015;29:1–7.
22. Hutanasu C, Sfarti C, Trifan A, Cojocariu C, Singeap AM, Spac A, Stanciu C. High levels of sterigmatocystin in patients with chronic liver diseases. Rev Med Chir Soc Med Nat Iasi. 2011;115:33–7.
23. Schroeder HW, Kelton WH. Production of sterigmatocystin by some species of the genus aspergillus and its toxicity to chicken embryos. Appl Microbiol. 1975;30:589–91.
24. Namgoong S, Kim NH. Roles of actin binding proteins in mammalian oocyte maturation and beyond. Cell Cycle. 2016;15:1830–43.
25. Muslin AJ, MacNicol AM, Williams LT. Raf-1 protein kinase is important for progesterone-induced Xenopus oocyte maturation and acts downstream of mos. Mol Cell Biol. 1993;13:4197–202.
26. Lan M, Han J, Pan MH, Wan X, Pan ZN, Sun SC. Melatonin protects against defects induced by deoxynivalenol during mouse oocyte maturation. J Pineal Res. 2018;65:e12477.
27. Viegas C, Nurme J, Pieckova E, Viegas S. Sterigmatocystin in foodstuffs and feed: aspects to consider. Mycology. 2018;11:91–104.
28. Sivakumar V, Thanislass J, Niranjali S, Devaraj H. Lipid peroxidation as a possible secondary mechanism of sterigmatocystin toxicity. Hum Exp Toxicol. 2001;20:398–403.
29. Shen L, Gaslonde T, Roullier C, Wang H, Bodin J, Poree FH, Ruprich-Robert G, Chapeland-Leclerc F. Functional characterization of the gata-type transcription factor pansdd in the filamentous fungus podospora anserina and its interplay with the Sterigmatocystin pathway. Appl Environ Microbiol. 2022;88:e0237821.
30. Xing C, Chen S, Wang Y, Pan Z, Zou Y, Sun S, Ren Z, Zhang Y. Glyphosate exposure deteriorates oocyte meiotic maturation via induction of organelle dysfunctions in pigs. J Anim Sci Biotechnol. 2022;13:80.
31. Wang YS, Yang SJ, Wan ZX, Shen A, Ahmad MJ, Chen MY, Huo LJ, Pan JH. Chlorothalonil exposure compromised mouse oocyte in vitro maturation through inducing oxidative stress and activating MAPK pathway. Ecotoxicol Environ Saf. 2024;273:116100.
32. Sreemannarayana O, Frohlich AA, Marquardt RR. Effects of repeated intraabdominal injections of sterigmatocystin on relative organ weights, concentration of serum and liver constituents, and histopathology of certain organs of the chick. Poult Sci. 1988;67:502–9.
33. Ezekiel CN, Abia WA, Braun D, Sarkanj B, Ayeni KI, Oyedele OA, Michael-Chikezie EC, Ezekiel VC, Mark BN, Ahuchaogu CP, et al. Mycotoxin exposure biomonitoring in breastfed and non-exclusively breastfed Nigerian children. Environ Int. 2022;158:106996.
34. Arce-Lopez B, Lizarraga E, Flores-Flores M, Irigoyen A, Gonzalez-Penas E. Development and validation of a methodology based on Captiva EMR-lipid clean-up and LC-MS/MS analysis for the simultaneous determination of mycotoxins in human plasma. Talanta. 2020;206:120193.
35. Tarazona AM, Rodriguez JI, Restrepo LF, Olivera-Angel M. Mitochondrial activity, distribution and segregation in bovine oocytes and in embryos produced in vitro. Reprod Domest Anim. 2006;41:5–11.
36. Egerszegi I, Alm H, Ratky J, Heleil B, Brussow KP, Torner H. Meiotic progression, mitochondrial features and fertilisation characteristics of porcine oocytes with different G6PDH activities. Reprod Fertil Dev. 2010;22:830–8.
37. Zhou W, Yang J, Zhang DI, Li F, Li G, Gu Y, Luo M. Role of Bcl-2/adenovirus E1B 19 kDa-interacting protein 3 in myocardial cells in diabetes. Exp Ther Med. 2015;10:67–73.
38. Balogh K, Kovesi B, Zandoki E, Kulcsar S, Ancsin Z, Erdelyi M, Dobolyi C, Bata-Vidacs I, Inotai K, Szekeres A, et al. Effect of sterigmatocystin or aflatoxin contaminated feed on lipid peroxidation and glutathione redox system and expression of glutathione redox system regulatory genes in broiler chicken. Antioxid (Basel). 2019;8(7):201.
39. Li X, Feng C, Sha H, Zhou T, Zou G, Liang H. Tandem mass tagging-based quantitative proteomics analysis reveals damage to the liver and brain of hypophthalmichthys molitrix exposed to acute hypoxia and reoxygenation. Antioxid (Basel). 2022;11(3):589.
40. Dupre A, Haccard O, Jessus C. Mos in the oocyte: how to use MAPK independently of growth factors and transcription to control meiotic divisions. J Signal Transduct. 2011;2011:350412.
41. Li GY, Li T, Fan B, Zheng YC, Ma TH. The D(1) dopamine receptor agonist, SKF83959, attenuates hydrogen peroxide-induced injury in RGC-5 cells involving the extracellular signal-regulated kinase/p38 pathways. Mol Vis. 2012;18:2882–95.
42. Zhang YL, Liu XM, Ji SY, Sha QQ, Zhang J, Fan HY. ERK1/2 activities are dispensable for oocyte growth but are required for meiotic maturation and pronuclear formation in mouse. J Genet Genomics. 2015;42:477–85.
43. Cai J, Wang J, Huang Y, Wu H, Xia T, Xiao J, Chen X, Li H, Qiu Y, Wang Y, et al. ERK/Drp1-dependent mitochondrial fission is involved in the MSC-induced drug resistance of T-cell acute lymphoblastic leukemia cells. Cell Death Dis. 2016;7:e2459.
44. Teng F, Xu Z, Chen J, Zheng G, Zheng G, Lv H, Wang Y, Wang L, Cheng X. DUSP1 induces apatinib resistance by activating the MAPK pathway in gastric cancer. Oncol Rep. 2018;40:1203–22.
45. Kho DH, Uddin MH, Chatterjee M, Vogt A, Raz A, Wu GS. GP78 cooperates with dual-specificity phosphatase 1 to stimulate epidermal growth factor receptor-mediated extracellular signal-regulated kinase signaling. Mol Cell Biol. 2019;39(11):e00485–18.
46. Fu XH, Chen CZ, Li S, Han DX, Wang YJ, Yuan B, Gao Y, Zhang JB, Jiang H. Dual-specificity phosphatase 1 regulates cell cycle progression and apoptosis in cumulus cells by affecting mitochondrial function, oxidative stress, and autophagy. Am J Physiol Cell Physiol. 2019;317:C1183–93.
47. Shi L, Wei X, Wu B, Yuan C, Li C, Dai Y, Chen J, Zhou F, Lin X, Zhang S. Molecular signatures correlated with poor ivf outcomes: insights from the mrna and lncrna expression of endometriotic granulosa cells. Front Endocrinol (Lausanne). 2022;13:825934.
48. Srinivas US, Tan BWQ, Vellayappan BA, Jeyasekharan AD. ROS and the DNA damage response in cancer. Redox Biol. 2019;25:101084.
49. Lu Z, Wan G, Guo H, Zhang X, Lu X. Protein phosphatase 1 inhibits p53 signaling by dephosphorylating and stabilizing Mdmx. Cell Signal. 2013;25:796–804.
50. Al-Zubaidi U, Adhikari D, Cinar O, Zhang QH, Yuen WS, Murphy MP, Rombauts L, Robker RL, Carroll J. Mitochondria-targeted therapeutics, MitoQ and BGP-15, reverse aging-associated meiotic spindle defects in mouse and human oocytes. Hum Reprod. 2021;36:771–84.
51. Liu M, Wu K, Wu Y. The emerging role of ferroptosis in female reproductive disorders. Biomed Pharmacother. 2023;166:115415.
52. Li Y, He Y, Cheng W, Zhou Z, Ni Z, Yu C. Double-edged roles of ferroptosis in endometriosis and endometriosis-related infertility. Cell Death Discov. 2023;9:306.
53. Chen M, Shi Z, Sun Y, Ning H, Gu X, Zhang L. Prospects for anti-tumor mechanism and potential clinical application based on glutathione peroxidase 4 mediated ferroptosis. Int J Mol Sci. 2023;24(2):1607.
54. Friedmann Angeli JP, Schneider M, Proneth B, Tyurina YY, Tyurin VA, Hammond VJ, Herbach N, Aichler M, Walch A, Eggenhofer E, et al. Inactivation of the ferroptosis regulator Gpx4 triggers acute renal failure in mice. Nat Cell Biol. 2014;16:1180–91.
55. Liu Y, Beyer A, Aebersold R. On the dependency of cellular protein levels on mrna abundance. Cell. 2016;165:535–50.
56. Buccitelli C, Selbach M. mRNAs, proteins and the emerging principles of gene expression control. Nat Rev Genet. 2020;21:630–44.
57. Wang F, Liu Y, Ni F, Jin J, Wu Y, Huang Y, Ye X, Shen X, Ying Y, Chen J, et al. BNC1 deficiency-triggered ferroptosis through the NF2-YAP pathway induces primary ovarian insufficiency. Nat Commun. 2022;13:5871.
58. Barrera G. Oxidative stress and lipid peroxidation products in cancer progression and therapy. ISRN Oncol. 2012;2012:137289.
59. Zingales V, Torriero N, Zanella L, Fernandez-Franzon M, Ruiz MJ, Esposito MR, Cimetta E. Development of an in vitro neuroblastoma 3D model and its application for sterigmatocystin-induced cytotoxicity testing. Food Chem Toxicol. 2021;157:112605.
60. Janke C, Bulinski JC. Post-translational regulation of the microtubule cytoskeleton: mechanisms and functions. Nat Rev Mol Cell Biol. 2011;12:773–86.
61. Al-Bassam J, Corbett KD. Alpha-tubulin acetylation from the inside out. Proc Natl Acad Sci U S A. 2012;109:19515–6.
62. Chen YT, Chen YF, Chiu WT, Liu KY, Liu YL, Chang JY, Chang HC, Shen MR. Microtubule-associated histone deacetylase 6 supports the calcium store sensor STIM1 in mediating malignant cell behaviors. Cancer Res. 2013;73:4500–9.
63. Hubbert C, Guardiola A, Shao R, Kawaguchi Y, Ito A, Nixon A, Yoshida M, Wang XF, Yao TP. HDAC6 is a microtubule-associated deacetylase. Nature. 2002;417:455–8.
64. Zou YJ, Shan MM, Wan X, Liu JC, Zhang KH, Ju JQ, Xing CH, Sun SC. Kinesin KIF15 regulates tubulin acetylation and spindle assembly checkpoint in mouse oocyte meiosis. Cell Mol Life Sci. 2022;79:422.

65. Li X, Liu X, Gao M, Han L, Qiu D, Wang H, Xiong B, Sun SC, Liu H, Gu L. HDAC3 promotes meiotic apparatus assembly in mouse oocytes by modulating tubulin acetylation. Development. 2017;144:3789–97.
66. Jeon HJ, Oh JS. RASSF1A regulates spindle organization by modulating tubulin acetylation via sirt2 and hdac6 in mouse oocytes. Front Cell Dev Biol. 2020;8:601972.
67. Wang R, Mercaitis OP, Jia L, Panettieri RA, Tang DD. Raf-1, actin dynamics, and abelson tyrosine kinase in human airway smooth muscle cells. Am J Respir Cell Mol Biol. 2013;48:172–8.
68. Wu X, Yin J, Simpson J, Kim KH, Gu S, Hong JH, Bayliss P, Backx PH, Neel BG, Araki T. Increased BRAF heterodimerization is the common pathogenic mechanism for noonan syndrome-associated RAF1 mutants. Mol Cell Biol. 2012;32:3872–90.
69. Luo X, Liu H, Guo H, Sun L, Gou K, Cui S. RAF1 mediates the FSH signaling pathway as a downstream molecule to stimulate estradiol synthesis and secretion in mouse ovarian granulosa cells. Ann Transl Med. 2022;10:314.

## Publisher's note